

Colored-Noise Kalman Filter for Vibration Mitigation of Position/Attitude Estimation Systems

Anjani Kumar*

Peritus Inc., 8800 Grand Oaks Circle, Suite 100, Tampa, FL 33637

John L. Crassidis†

University at Buffalo, State University of New York, Amherst, NY 14260-4400

A colored-noise Kalman filter is designed to diminish the error effects caused by sensors placed on vibrating structures. This paper deals with sensors that are used to estimate position, attitude or both. Here we focus on a vision-based system, which uses a set of light-emitting diode beacons with a focal plane detector to determine line-of-sight measurements. Estimation of both position and attitude is possible with this system. Vibrational effects are added to the beacon locations and a colored-noise filter is designed to mitigate the effects of the beacon movements on state estimation. A sensitivity study is conducted for this paper work, where the effects of beacon location errors on the estimation of a vehicle's position and attitude are examined. Beacon location variation is introduced into the standard vision-based navigation problem as second-order vibration noise. Further, an error in the process-noise covariance is assumed and its effect on the estimated quantity is observed. Different magnitudes of vibration are added to the beacons position and the robustness properties of the colored-noise filter is analyzed. Results indicate that the colored-noise filter provides significant improvements over a filter that does not account for vibrational effects.

I. Introduction

Various sensors can be used for vehicle systems that require position and/or attitude knowledge. The choice of sensors is mainly dictated by the particular application. Oftentimes the position and attitude determination problems are decoupled. For example, in most spacecraft applications position sensors, such as standard Global Positioning System (GPS) receivers, are used to determine the orbital position while attitude sensors, such as star trackers, are used to determine the orientation. Sometimes, one sensor package can be used for both. For example, the International Space Station uses GPS to determine both position and attitude.¹ For this application, carrier-based measurements must be employed with multiple antennas for attitude determination, which isn't necessarily required for position determination. Other applications involve using GPS with an Inertial Navigation System (INS), consisting of gyros and accelerometers, to determine an aircraft's absolute position and attitude.² Vision-based systems for robotic navigation are now commonplace,³ and have even been used for automatic rendezvous and docking system applications.⁴ With the advent of greater signal processing capabilities coupled with smaller and cheaper sensor technology, the amount of sensors available for attitude and position estimation within an autonomous operations framework will surely grow in the future.

Most studies on sensors focus on errors that degrade state and parameter estimation accuracies, which has been an issue for many years now. For example, sensitivity studies on random and systematic errors in sensors provide a mechanism to discovery possible anomalous characteristics or problems at an early stage.⁵ Placement of sensor locations is also important to overall estimation performance. The traditional sensor-placement problem is based on static process conditions, which can be extended to linear dynamic processes.⁶ Another approach to determine optimal sensor locations is by minimizing the condition number

*Software Developer, Email: anjani604@gmail.com.

†Professor, Department of Mechanical & Aerospace Engineering. Email: johnc@eng.buffalo.edu. Associate Fellow AIAA.

of the observability matrix.⁷ Reference 8 presents an observability analysis for determining both position and attitude from line-of-sight (LOS) measurements. When three or more LOS measurements are available the associated attitude/position covariance has full rank in most cases, and a unique solution for attitude and position exists for four or more LOS measurements. An interesting scenario involves the case where the endpoints of the position vectors of the sensors are connected by a straight line, which leads to an unobservable system, not matter how LOS measurements are available. All of these studies can be used to quantify the expected performance using various sensors through systematic design tools.

Another issue that clearly affects the performance of position/attitude determination systems is sensor movements. These movements can arise from a number possibilities, but the most common are from vibrational effects where sensors are placed on flexible structures. For example, GPS antennae have been placed on spacecraft solar arrays, which are very flexible and can lead to errors of several degrees in attitude performance.⁹ Reference 10 shows actual flight tests results of using GPS to determine the attitude of an aircraft. Two of the GPS antennae are placed on the wing tips, which can have a deflection of almost 10 cm steady-state for the particular aircraft used. Another antenna of the main fuselage was also assumed to deflect, although not as much as the wing antennae. In addition to estimating attitude, the effect of the baseline deflections was also studied. Deflection in the symmetric up-down bending of the wings is assumed, so that only one parameter needed to be estimated for the baseline correction due to flexible motion of the wing. The deflection was not determined by the estimation process though. Rather, various values of the deflection scalar variable were studied and it was determined that a nonzero value did provide better estimates when compared to the onboard inertial navigation solution.

In this paper an approach is introduced to mitigate the errors induced from sensors placed on flexible structures. The approach relies on a colored-noise Kalman filter, because the noise on the measurements is no longer Gaussian due to the flexible motion of the sensors. Colored-noise filters are design by incorporating *shaping filters* that are driven by zero-mean Gaussian noise processes.¹¹ The filter state is augmented to include the shaping filter states, but the overall structure of the colored-noise filter follows the Kalman structure with the exception when a correlation exists between that measurement noise and process noise. Here we employ a vision-based system that provides LOS measurements.¹² A thirteen-state extended Kalman filter (EKF) is first designed to estimate position, orientation, linear velocity and angular velocity. Beacon location variation is introduced into the standard vision-based estimation problem as second-order vibration noise. The effects of the vibration noise are mitigated by using a forty-nine colored-noise filter. Further, an error in the covariance is assumed and its effect on the estimated quantity is observed. Different magnitudes of vibration are added to the beacons position and the robustness properties of the colored-noise filter is analyzed. Simulation results will show the effectiveness of the colored-noise filter using a realistic sensor based on vision technology.¹²

The organization of this paper is as follows. First, the basic sensor systems used for the work are described, which also includes the measurement covariance. Then a review of the quaternion attitude parameterization is given. Next, the EKF for position and attitude estimation using the sensor systems is derived. A discrete-time propagation of the states and covariance is used in this work. Then, the colored-noise EKF is developed, which incorporates a vibration model for the sensor movements. Finally, simulation results are presented that show comparisons between the EKFs with and without the colored-noise model.

II. Sensor Systems

In this section, the main sensor used to obtain the LOS measurements and gyro model are summarized. As previously mentioned the colored-noise Kalman filter approach shown in the paper is applicable to any sensor system that involves deformation of the structure where the sensor is located. In this paper a vision-based (VISNAV) navigation system is studied because it can be used to determine both position and attitude. The design methodology for other sensor systems can easily be incorporated from the basic structure of the colored-noise filter developed in this paper.

A. Vision-Based Navigation

The VISNAV system was first introduced by Junkins, Hughes, Wazni and Pariyapong in Ref. 12. Gunman et al. presented detailed work with the digital signal processing (DSP) optical navigation sensor in Ref. 13. Target beacons are fixed in the target vehicle with known position in some reference frame and an optical

sensor is attached in the chase vehicle. The sensor is made up of a Position Sensing Diode (PSD) placed in the focal plane of a wide angle lens. Current imbalances are produced when the silicon area of the PSD is illuminated by a beacon focused by the lens. The PSD photodetector, combined with an omnidirectional lens, is an analog detector that inherently captures incident light, from which a LOS vector can be determined. PSDs have rise times of about five microseconds, making them relatively fast when compared even to high speed cameras. The idea behind the concept of intelligent vision is that the PSD can be used to see only specific light sources. This can be done by frequency domain structuring of the target lights and with analog signal processing. With this approach, light sources, called beacons are used to establish the LOS vector. Each beacon is comprised of a series of Light Emitting Diodes (LEDs) which radiate energy over nearly a hemisphere. A beacon orchestration process distinguishes one beacon from another and an elaborate modulation/demodulation technique washes out the effects of surrounding environmental light sources.

There are many applications of the VISNAV system. Relative navigation and attitude estimation of spacecraft flying in formation with the use of the VISNAV system is shown in Ref. 14. The approach uses information from the optical sensor to provide a LOS vector from the chief spacecraft to the secondary satellite. The overall system provides a reliable and autonomous relative navigation and attitude determination system, employing relatively simple electronic circuits with modest digital signal processing requirements and is fully independent of any external systems. State estimation is achieved through a Kalman filter model coupled with a relative orbital model and gyro measurements that drive a kinematics model. Valasek et al. present the use of the VISNAV system for autonomous aerial refueling in Ref. 15. This paper presented the preliminary design of an accurate and reliable vision-based sensor and controller for autonomous aerial refueling of unmanned air vehicles. Results indicate that the integrated sensor and controller provide precise aerial refueling with good disturbance rejection characteristics.

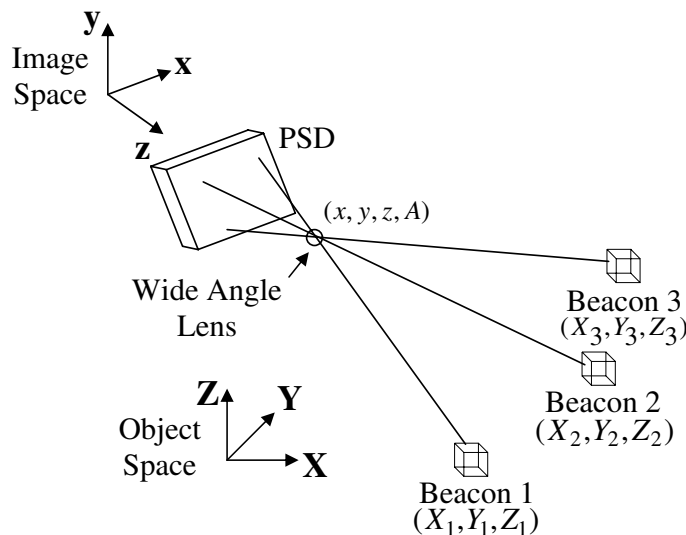


Figure 1. Vision-Based Navigation System

Photogrammetry is the technique of measuring objects (2D or 3D) from photographic images or LOS measurements. Photogrammetry can generally be divided into two categories: far range photogrammetry with camera distance settings to infinity (commonly used in star cameras), and close-range photogrammetry with camera distance settings to finite values. In general close-range photogrammetry can be used to determine both the attitude and position of an object, while far range photogrammetry can only be used to determine attitude. The VISNAV system comprises an optical sensor of a new kind combined with specific light sources (beacons), which can be used for close-range photogrammetry-type applications. The relationship between the attitude/position and the observations used in photogrammetry involves a set of colinearity equations, which are reviewed in this section. Figure 1 shows a schematic of the typical quantities involved in basic photogrammetry from LOS measurements, derived from light beacons in this case. It is assumed that the location of the sensor focal plane is known within the image-space coordinate system, which is usually obtained through calibration. If we choose the z -axis of the sensor coordinate system to be directed outward along the boresight, then given object space and image space coordinate frames, the ideal object to image

space projective transformation (noiseless) can be written as follows:¹⁶

$$\chi_i = -f \frac{A_{11}(X_i - x) + A_{12}(Y_i - y) + A_{13}(Z_i - z)}{A_{31}(X_i - x) + A_{32}(Y_i - y) + A_{33}(Z_i - z)}, \quad i = 1, 2, \dots, N \quad (1a)$$

$$\gamma_i = -f \frac{A_{21}(X_i - x) + A_{22}(Y_i - y) + A_{23}(Z_i - z)}{A_{31}(X_i - x) + A_{32}(Y_i - y) + A_{33}(Z_i - z)}, \quad i = 1, 2, \dots, N \quad (1b)$$

where N is the total number of observations, (χ_i, γ_i) are the image space observations for the i^{th} LOS, (X_i, Y_i, Z_i) are the known object space locations of the i^{th} beacon, (x, y, z) are the unknown object space location of the sensor, f is the known focal length, and A_{jk} are the unknown coefficients of the attitude matrix, A , associated to the orientation from the object plane to the image plane. The goal of the *inverse problem* is given observations (χ_i, γ_i) and object space locations (X_i, Y_i, Z_i) , for $i = 1, 2, \dots, N$, determine the attitude (A) and position (x, y, z) .

The observation can be reconstructed in unit vector form as

$$\mathbf{b}_i = A \mathbf{r}_i, \quad i = 1, 2, \dots, N \quad (2)$$

where

$$\mathbf{b}_i \equiv \frac{1}{\sqrt{f^2 + \chi_i^2 + \gamma_i^2}} \begin{bmatrix} -\chi_i \\ -\gamma_i \\ f \end{bmatrix} \quad (3a)$$

$$\mathbf{r}_i \equiv \frac{1}{\sqrt{(X_i - x)^2 + (Y_i - y)^2 + (Z_i - z)^2}} \begin{bmatrix} X_i - x \\ Y_i - y \\ Z_i - z \end{bmatrix} \quad (3b)$$

When measurement noise is present, the measurement model becomes

$$\tilde{\mathbf{b}}_i = A \mathbf{r}_i + \mathbf{v}_i \quad (4)$$

where $\tilde{\mathbf{b}}_i$ denotes the i^{th} measurement, and the sensor error \mathbf{v}_i is approximately Gaussian which satisfies¹⁷

$$E \{ \mathbf{v}_i \} = \mathbf{0} \quad (5a)$$

$$\mathcal{R}_i \equiv E \{ \mathbf{v}_i \mathbf{v}_i^T \} = J_i R_i^{\text{FOCAL}} J_i^T \quad (5b)$$

where $E \{ \}$ denotes expectation and

$$J_i \equiv \frac{1}{\sqrt{1 + \chi_i^2 + \gamma_i^2}} \begin{bmatrix} -1 & 0 \\ 0 & -1 \\ 0 & 0 \end{bmatrix} - \frac{1}{1 + \chi_i^2 + \gamma_i^2} \mathbf{b}_i \begin{bmatrix} \chi_i & \gamma_i \end{bmatrix} \quad (6a)$$

$$R_i^{\text{FOCAL}} = \frac{\sigma_i^2}{1 + d(\chi_i^2 + \gamma_i^2)} \begin{bmatrix} (1 + d\chi_i^2)^2 & (d\chi_i\gamma_i)^2 \\ (d\chi_i\gamma_i)^2 & (1 + d\gamma_i^2)^2 \end{bmatrix} \quad (6b)$$

where σ_i^2 is the variance of the measurement errors associated with χ_i and γ_i , and d is on the order of one. Note that as χ_i or γ_i increases then the individual components of R_i^{FOCAL} increase, which realistically shows that the errors increase as the observation moves away from the boresight. As stated in Ref. 18, the covariance model is a function of the true variables χ_i and γ_i , which are never available in practice. However, using the measurements themselves or estimated quantities from the EKF leads to only second-order error effects.

Equation (5) does not make the small field-of-view (FOV) assumption, which is more useful for the VISNAV sensor since it incorporates a wide angle lens. Rather, the assumption leading to Eq. (5) is that the measurement noise is “small” compared to the signal, so that a first-order Taylor series expansion accurately captures the error process (see Ref. 17 for details). However, there may be circumstances where all the LOS measurements are within a small FOV. For this case Shuster¹⁹ has shown that nearly all the probability of

the errors is concentrated on a very small area about the direction of $\mathbf{A}\mathbf{r}_i$, so the sphere containing that point can be approximated by a tangent plane, characterized by

$$E\{\mathbf{v}_i\} = \mathbf{0} \quad (7a)$$

$$\mathcal{R}_i = \sigma_i^2 (I_{3 \times 3} - \mathbf{b}_i \mathbf{b}_i^T) \quad (7b)$$

where $I_{3 \times 3}$ denotes a 3×3 identity matrix. Equation (7b) approximates Eq. (5b) well under the small FOV assumption, but can lead to fairly large estimation errors if this assumption is not valid.¹⁷

The covariance matrices in Eqs. (5b) and (7b) are both singular, which leads to a singularity in the calculation of the Kalman gain. Shuster¹⁸ first showed that the singular covariance matrix in Eq. (7b) can be effectively replaced with a nonsingular diagonal matrix made up of σ_i^2 terms. This concept is expanded in Ref. 17 to include the general covariance shown by Eq. (5b). For each measurement, the matrix used to make up the EKF measurement-error covariance matrix is given by a rank-one update to \mathcal{R}_i :

$$R_i = \mathcal{R}_i + \frac{1}{2} \text{trace}(\mathcal{R}_i) \mathbf{b}_i \mathbf{b}_i^T \quad (8)$$

This matrix is always nonsingular.¹⁷ If Eq. (7b) is used in Eq. (8) then we have $R_i = \sigma_i^2 I_{3 \times 3}$. Finally, concatenating all R_i matrices for the available LOS measurements at time-step t_k into a block diagonal matrix leads to the EKF measurement covariance matrix, denoted by R_k .

B. Gyro Model

A common sensor that measures the angular rate is a rate-integrating gyro. For this sensor, a widely used three-axis continuous-time model is given by²⁰

$$\dot{\tilde{\boldsymbol{\omega}}} = \boldsymbol{\omega} + \boldsymbol{\beta} + \boldsymbol{\eta}_v \quad (9a)$$

$$\dot{\boldsymbol{\beta}} = \boldsymbol{\eta}_u \quad (9b)$$

where $\boldsymbol{\omega}$ is the three-component true angular-rate vector, $\tilde{\boldsymbol{\omega}}$ is the measured rate, $\boldsymbol{\beta}$ is the drift, and $\boldsymbol{\eta}_v$ and $\boldsymbol{\eta}_u$ are independent zero-mean Gaussian white-noise processes with

$$E\{\boldsymbol{\eta}_v(t)\boldsymbol{\eta}_v^T(\tau)\} = \sigma_v^2 \delta(t - \tau) I_{3 \times 3} \quad (10a)$$

$$E\{\boldsymbol{\eta}_u(t)\boldsymbol{\eta}_u^T(\tau)\} = \sigma_u^2 \delta(t - \tau) I_{3 \times 3} \quad (10b)$$

where $\delta(t - \tau)$ is the Dirac delta function. For simulation purposes, discrete-time gyro measurements can be generated using the following equations:²¹

$$\tilde{\boldsymbol{\omega}}_{k+1} = \boldsymbol{\omega}_{k+1} + \frac{1}{2}[\boldsymbol{\beta}_{k+1} + \boldsymbol{\beta}_k] + \left[\frac{\sigma_v^2}{\Delta t} + \frac{1}{12} \sigma_u^2 \Delta t \right]^{1/2} \mathbf{N}_v \quad (11a)$$

$$\boldsymbol{\beta}_{k+1} = \boldsymbol{\beta}_k + \sigma_u \Delta t^{1/2} \mathbf{N}_u \quad (11b)$$

where the subscript k denotes the k^{th} time-step, Δt is the gyro sampling interval, and \mathbf{N}_v and \mathbf{N}_u are zero-mean Gaussian white-noise processes with covariance each given by the identity matrix.

III. Attitude Parameterization

Several parameterizations of the attitude are possible.²² In this paper the quaternion parameterization is used, which is a four-dimensional vector, defined as

$$\mathbf{q} \equiv \begin{bmatrix} \boldsymbol{\rho} \\ q_4 \end{bmatrix} \quad (12)$$

with

$$\boldsymbol{\rho} \equiv [q_1 \ q_2 \ q_3]^T = \mathbf{e} \sin(\vartheta/2) \quad (13a)$$

$$q_4 = \cos(\vartheta/2) \quad (13b)$$

where \mathbf{e} is the unit Euler axis and ϑ is the rotation angle. Since a four-dimensional vector is used to describe three dimensions, the quaternion components cannot be independent of each other. The quaternion satisfies a single constraint given by $\mathbf{q}^T \mathbf{q} = 1$. The attitude matrix is related to the quaternion by

$$A(\mathbf{q}) = (q_4^2 - \|\boldsymbol{\rho}\|^2) I_{3 \times 3} + 2\boldsymbol{\rho} \boldsymbol{\rho}^T - 2q_4[\boldsymbol{\rho} \times] = \Xi^T(\mathbf{q})\Psi(\mathbf{q}) \quad (14)$$

where $I_{3 \times 3}$ is a 3×3 identity matrix and

$$\Xi(\mathbf{q}) \equiv \begin{bmatrix} q_4 I_{3 \times 3} + [\boldsymbol{\rho} \times] \\ -\boldsymbol{\rho}^T \end{bmatrix} \quad (15a)$$

$$\Psi(\mathbf{q}) \equiv \begin{bmatrix} q_4 I_{3 \times 3} - [\boldsymbol{\rho} \times] \\ -\boldsymbol{\rho}^T \end{bmatrix} \quad (15b)$$

Also, $[\boldsymbol{\rho} \times]$ is the cross-product matrix defined by

$$[\boldsymbol{\rho} \times] \equiv \begin{bmatrix} 0 & -q_3 & q_2 \\ q_3 & 0 & -q_1 \\ -q_2 & q_1 & 0 \end{bmatrix} \quad (16)$$

For small angles the vector part of the quaternion is approximately equal to half angles,²² which will be used later.

The quaternion kinematics equation is given by

$$\dot{\mathbf{q}} = \frac{1}{2} \Xi(\mathbf{q}) \boldsymbol{\omega} = \frac{1}{2} \Omega(\boldsymbol{\omega}) \mathbf{q} \quad (17)$$

where

$$\Omega(\boldsymbol{\omega}) \equiv \begin{bmatrix} -[\boldsymbol{\omega} \times] & \boldsymbol{\omega} \\ -\boldsymbol{\omega}^T & 0 \end{bmatrix} \quad (18)$$

A major advantage of using the quaternion is that the kinematics equation is linear in the quaternion and is also free of singularities. Another advantage of the quaternion is that successive rotations can be accomplished using quaternion multiplication. Here the convention of Ref. 23 is adopted, where the quaternions are multiplied in the same order as the attitude matrix multiplication, in contrast to the usual convention established by Hamilton.²⁴ A successive rotation is written using

$$A(\mathbf{q}')A(\mathbf{q}) = A(\mathbf{q}' \otimes \mathbf{q}) \quad (19)$$

The composition of the quaternions is bilinear, with

$$\mathbf{q}' \otimes \mathbf{q} = \begin{bmatrix} \Psi(\mathbf{q}') & \mathbf{q}' \\ \Xi(\mathbf{q}) & \mathbf{q} \end{bmatrix} \mathbf{q}' \quad (20)$$

Also, the inverse quaternion is defined by

$$\mathbf{q}^{-1} \equiv \begin{bmatrix} -\boldsymbol{\rho} \\ q_4 \end{bmatrix} \quad (21)$$

Note that $\mathbf{q} \otimes \mathbf{q}^{-1} = [0 \ 0 \ 0 \ 1]^T$, which is the identity quaternion.

IV. Kalman Filter for Position and Attitude Estimation

The Kalman filter is used as the foundation for position and attitude estimation. The quaternion linearization process follows the multiplicative approach summarized in Refs. 23 and 25, which is briefly reviewed here.

$$\delta \mathbf{q} = \mathbf{q} \otimes \hat{\mathbf{q}}^{-1} \quad (22)$$

with \mathbf{q} is true quaternion, $\hat{\mathbf{q}}$ is the estimated quaternion and $\delta\mathbf{q} \equiv [\delta\boldsymbol{\rho}^T \delta q_4]^T$. Taking the time derivative of Eq. (22) gives²³

$$\delta\dot{\mathbf{q}} = \begin{bmatrix} [\hat{\boldsymbol{\omega}} \times] \delta\boldsymbol{\rho} \\ 0 \end{bmatrix} + \frac{1}{2} \begin{bmatrix} \delta\boldsymbol{\omega} \\ 0 \end{bmatrix} \otimes \delta\mathbf{q} \quad (23)$$

with $\hat{\boldsymbol{\omega}} = \tilde{\boldsymbol{\omega}} - \hat{\boldsymbol{\beta}}$, where $\hat{\boldsymbol{\beta}}$ is estimated gyro bias vector, and $\delta\boldsymbol{\omega} = \boldsymbol{\omega} - \hat{\boldsymbol{\omega}}$. The nonlinear term appears only in the second term at the right-hand side of Eq. (23). Its first order approximation is given as

$$\frac{1}{2} \begin{bmatrix} \delta\boldsymbol{\omega} \\ 0 \end{bmatrix} \otimes \delta\mathbf{q} \approx \frac{1}{2} \begin{bmatrix} \delta\boldsymbol{\omega} \\ 0 \end{bmatrix} \quad (24)$$

Using the small angle approximation $\delta\boldsymbol{\rho} = \delta\boldsymbol{\alpha}/2$, where $\boldsymbol{\alpha}$ has components of roll, pitch and yaw angle errors for any rotation sequence, and substituting the gyro and estimate models into $\delta\boldsymbol{\omega}$ leads to

$$\delta\dot{\boldsymbol{\alpha}} = -[\hat{\boldsymbol{\omega}} \times] \delta\boldsymbol{\alpha} - (\Delta\boldsymbol{\beta} + \boldsymbol{\eta}_v) \quad (25)$$

where $\Delta\boldsymbol{\beta} = \boldsymbol{\beta} - \hat{\boldsymbol{\beta}}$. The linearization process of the measurement output for the attitude portion can be found in Ref. 23, which is not repeated here.

The state vector consists of the position vector $\mathbf{p} \equiv [x \ y \ z]^T$, the velocity vector $\mathbf{v} \equiv [\dot{x} \ \dot{y} \ \dot{z}]^T$, the quaternion \mathbf{q} and the gyro bias vector $\boldsymbol{\beta}$:

$$\mathbf{x} = [\mathbf{p}^T \ \mathbf{v}^T \ \mathbf{q}^T \ \boldsymbol{\beta}^T]^T \quad (26)$$

The dynamics model of the linear velocity follows

$$\dot{\mathbf{v}} = \boldsymbol{\eta}_a \quad (27)$$

where $\boldsymbol{\eta}_a$ is a zero-mean Gaussian noise process with spectral density given by $\sigma_a^2 I_{3 \times 3}$. The error-dynamics are given by

$$\Delta\dot{\mathbf{x}} = F(\hat{\mathbf{x}}, t) \Delta\mathbf{x} + G \mathbf{w} \quad (28)$$

where

$$\Delta\mathbf{x} = [\Delta\mathbf{p}^T \ \Delta\mathbf{v}^T \ \delta\boldsymbol{\alpha}^T \ \Delta\boldsymbol{\beta}^T]^T \quad (29a)$$

$$\mathbf{w} = [\boldsymbol{\eta}_a^T \ \boldsymbol{\eta}_v^T \ \boldsymbol{\eta}_u^T]^T \quad (29b)$$

$$F(\hat{\mathbf{x}}, t) = \begin{bmatrix} 0_{3 \times 3} & I_{3 \times 3} & 0_{3 \times 3} & 0_{3 \times 3} \\ 0_{3 \times 3} & 0_{3 \times 3} & 0_{3 \times 3} & 0_{3 \times 3} \\ 0_{3 \times 3} & 0_{3 \times 3} & -[\hat{\boldsymbol{\omega}} \times] & -I_{3 \times 3} \\ 0_{3 \times 3} & 0_{3 \times 3} & 0_{3 \times 3} & 0_{3 \times 3} \end{bmatrix} \quad (29c)$$

$$G = \begin{bmatrix} 0_{3 \times 3} & 0_{3 \times 3} & 0_{3 \times 3} \\ I_{3 \times 3} & 0_{3 \times 3} & 0_{3 \times 3} \\ 0_{3 \times 3} & -I_{3 \times 3} & 0_{3 \times 3} \\ 0_{3 \times 3} & 0_{3 \times 3} & I_{3 \times 3} \end{bmatrix} \quad (29d)$$

with $\Delta\mathbf{p} = \mathbf{p} - \hat{\mathbf{p}}$ and $\Delta\mathbf{v} = \mathbf{v} - \hat{\mathbf{v}}$, where $\hat{\mathbf{p}}$ and $\hat{\mathbf{v}}$ are the position and velocity estimates, respectively.

A summary of the Kalman filter for position and attitude estimation is given by Table 1. The process noise spectral density matrix is given by

$$Q = \begin{bmatrix} \sigma_a^2 I_{3 \times 3} & 0_{3 \times 3} & 0_{3 \times 3} \\ 0_{3 \times 3} & \sigma_v^2 I_{3 \times 3} & 0_{3 \times 3} \\ 0_{3 \times 3} & 0_{3 \times 3} & \sigma_u^2 I_{3 \times 3} \end{bmatrix} \quad (30)$$

All quantities with a superscript + denote updated values and all quantities with a superscript - denote propagated values. It is assumed for simplicity that the gyros and VISNAV sensor are sampled at the same

Table 1. Extended Kalman Filter for Position and Attitude Estimation

Model	$\dot{\mathbf{x}} = \mathbf{f}(\mathbf{x}, \tilde{\boldsymbol{\omega}}, t) + G \mathbf{w}, \quad \mathbf{w} \sim N(\mathbf{0}, Q)$ $\tilde{\mathbf{y}}_k = \begin{bmatrix} A(\mathbf{q})\mathbf{r}_1 \\ A(\mathbf{q})\mathbf{r}_2 \\ \vdots \\ A(\mathbf{q})\mathbf{r}_N \end{bmatrix} \Big _{t_k} + \begin{bmatrix} \mathbf{v}_1 \\ \mathbf{v}_2 \\ \vdots \\ \mathbf{v}_N \end{bmatrix} \Big _{t_k} \equiv \mathbf{h}_k(\hat{\mathbf{x}}_k) + \mathbf{v}_k, \quad \mathbf{v}_k \sim N(\mathbf{0}, R_k)$
Initialize	$\hat{\mathbf{p}}(t_0) = \hat{\mathbf{p}}_0, \quad \hat{\mathbf{v}}(t_0) = \hat{\mathbf{v}}_0, \quad \hat{\mathbf{q}}(t_0) = \hat{\mathbf{q}}_0, \quad \hat{\boldsymbol{\beta}}(t_0) = \hat{\boldsymbol{\beta}}_0$ $P(t_0) = P_0$
Gain	$K_k = P_k^- H_k^T(\hat{\mathbf{x}}_k^-) [H_k(\hat{\mathbf{x}}_k^-) P_k^- H_k^T(\hat{\mathbf{x}}_k^-) + R_k]^{-1}$
Update	$P_k^+ = [I - K_k H_k(\hat{\mathbf{x}}_k^-)] P_k^-$ $\Delta \hat{\mathbf{x}}_k^+ = K_k [\tilde{\mathbf{y}}_k - \mathbf{h}_k(\hat{\mathbf{x}}_k^-)]$ $\Delta \hat{\mathbf{x}}_k^+ \equiv \begin{bmatrix} \Delta \hat{\mathbf{p}}_k^{+T} & \Delta \hat{\mathbf{v}}_k^{+T} & \delta \hat{\boldsymbol{\alpha}}_k^{+T} & \Delta \hat{\boldsymbol{\beta}}_k^{+T} \end{bmatrix}^T$ $\mathbf{h}_k(\hat{\mathbf{x}}_k^-) = \begin{bmatrix} A(\hat{\mathbf{q}}^-)\mathbf{r}_1 \\ A(\hat{\mathbf{q}}^-)\mathbf{r}_2 \\ \vdots \\ A(\hat{\mathbf{q}}^-)\mathbf{r}_N \end{bmatrix} \Big _{t_k}$ $\hat{\mathbf{p}}_k^+ = \hat{\mathbf{p}}_k^- + \Delta \hat{\mathbf{p}}_k^+$ $\hat{\mathbf{v}}_k^+ = \hat{\mathbf{v}}_k^- + \Delta \hat{\mathbf{v}}_k^+$ $\hat{\mathbf{q}}_k^+ = \hat{\mathbf{q}}_k^- + \frac{1}{2} \Xi(\hat{\mathbf{q}}_k^-) \delta \hat{\boldsymbol{\alpha}}_k^+, \quad \text{re-normalize quaternion}$ $\hat{\boldsymbol{\beta}}_k^+ = \hat{\boldsymbol{\beta}}_k^- + \Delta \hat{\boldsymbol{\beta}}_k^+$
Propagation	$\hat{\mathbf{p}}_{k+1}^- = \hat{\mathbf{p}}_k^+ + \hat{\mathbf{v}}_k^+ \Delta t$ $\hat{\mathbf{v}}_{k+1}^- = \hat{\mathbf{v}}_k^+$ $\hat{\boldsymbol{\omega}}_k^+ = \tilde{\boldsymbol{\omega}}_k - \hat{\boldsymbol{\beta}}_k^+$ $\hat{\mathbf{q}}_{k+1}^- = \bar{\Omega}(\hat{\boldsymbol{\omega}}_k^+) \hat{\mathbf{q}}_k^+$ $\hat{\boldsymbol{\beta}}_{k+1}^- = \hat{\boldsymbol{\beta}}_k^+$ $P_{k+1}^- = \Phi_k P_k^+ \Phi_k^T + Q$

rates, although this does not need to be true in general. The matrix P denotes the state error-covariance.

The sensitivity matrix is given by

$$H_k(\hat{\mathbf{x}}_k^-) = \left[\begin{array}{cccc} \frac{\partial \hat{\mathbf{b}}_1^-}{\partial \hat{\mathbf{p}}^-} & 0_{3 \times 3} & [A(\hat{\mathbf{q}}^-) \hat{\mathbf{r}}_1^- \times] & 0_{3 \times 3} \\ \vdots & \vdots & \vdots & \vdots \\ \frac{\partial \hat{\mathbf{b}}_N^-}{\partial \hat{\mathbf{p}}^-} & 0_{3 \times 3} & [A(\hat{\mathbf{q}}^-) \hat{\mathbf{r}}_N^- \times] & 0_{3 \times 3} \end{array} \right]_{t_k} \quad (31)$$

where $\hat{\mathbf{r}}_i^-$ is given by Eq. (3b) evaluated at $\hat{\mathbf{p}}^- \equiv [\hat{x}^- \ \hat{y}^- \ \hat{z}^-]^T$ and the partial matrix $\partial \hat{\mathbf{b}}_i^- / \partial \hat{\mathbf{p}}^-$ is given by

$$\frac{\partial \hat{\mathbf{b}}_i^-}{\partial \hat{\mathbf{p}}^-} = A(\hat{\mathbf{q}}^-) \frac{\partial \hat{\mathbf{r}}_i^-}{\partial \hat{\mathbf{p}}^-} \quad (32)$$

where

$$\frac{\partial \hat{\mathbf{r}}_i^-}{\partial \hat{\mathbf{p}}^-} = \frac{1}{\hat{s}_i^-} \left[\begin{array}{ccc} -[(Y_i - \hat{y}^-)^2 + (Z_i - \hat{z}^-)^2] & (X_i - \hat{x}^-)(Y_i - \hat{y}^-) & (X_i - \hat{x}^-)(Z_i - \hat{z}^-) \\ (X_i - \hat{x}^-)(Y_i - \hat{y}^-) & -[(X_i - \hat{x}^-)^2 + (Z_i - \hat{z}^-)^2] & (Y_i - \hat{y}^-)(Z_i - \hat{z}^-) \\ (X_i - \hat{x}^-)(Z_i - \hat{z}^-) & (Y_i - \hat{y}^-)(Z_i - \hat{z}^-) & -[(X_i - \hat{x}^-)^2 + (Y_i - \hat{y}^-)^2] \end{array} \right] \quad (33)$$

with $\hat{s}_i^- \equiv [(X_i - \hat{x}^-)^2 + (Y_i - \hat{y}^-)^2 + (Z_i - \hat{z}^-)^2]^{3/2}$.

The closed-form solution for the quaternion propagation is used, where $\bar{\Omega}(\hat{\omega}_k^+)$ is given by²⁶

$$\bar{\Omega}(\hat{\omega}_k^+) \equiv \left[\begin{array}{cc} \cos(\frac{1}{2} \|\hat{\omega}_k^+\| \Delta t) I_{3 \times 3} - [\hat{\psi}_k^+ \times] & \hat{\psi}_k^+ \\ -\hat{\psi}_k^{+T} & \cos(\frac{1}{2} \|\hat{\omega}_k^+\| \Delta t) \end{array} \right] \quad (34)$$

with

$$\hat{\psi}_k^+ \equiv \frac{\sin(\frac{1}{2} \|\hat{\omega}_k^+\| \Delta t) \hat{\omega}_k^+}{\|\hat{\omega}_k^+\|} \quad (35)$$

Also, a discrete-time propagation of the covariance is also used, where the state transition matrix is given by

$$\Phi = \left[\begin{array}{cccc} I_{3 \times 3} & \Delta t I_{3 \times 3} & 0_{3 \times 3} & 0_{3 \times 3} \\ 0_{3 \times 3} & I_{3 \times 3} & 0_{3 \times 3} & 0_{3 \times 3} \\ 0_{3 \times 3} & 0_{3 \times 3} & \Phi_{33} & \Phi_{34} \\ 0_{3 \times 3} & 0_{3 \times 3} & 0_{3 \times 3} & I_{3 \times 3} \end{array} \right] \quad (36)$$

where

$$\Phi_{33} = I_{3 \times 3} - [\hat{\omega} \times] \frac{\sin(\|\hat{\omega}\| \Delta t)}{\|\hat{\omega}\|} + [\hat{\omega} \times]^2 \frac{\{1 - \cos(\|\hat{\omega}\| \Delta t)\}}{\|\hat{\omega}\|^2} \quad (37a)$$

$$\Phi_{34} = [\hat{\omega} \times] \frac{\{1 - \cos(\|\hat{\omega}\| \Delta t)\}}{\|\hat{\omega}\|^2} - I_{3 \times 3} \Delta t - [\hat{\omega} \times]^2 \frac{\{\|\hat{\omega}\| \Delta t - \sin(\|\hat{\omega}\| \Delta t)\}}{\|\hat{\omega}\|^3} \quad (37b)$$

The discrete-time process noise covariance is given by

$$\mathcal{Q} = \left[\begin{array}{ccc} \sigma_a^2 \Delta t I_{3 \times 3} & 0_{3 \times 3} & 0_{3 \times 3} \\ 0_{3 \times 3} & \left(\sigma_v^2 \Delta t + \frac{1}{3} \sigma_u^2 \Delta t^3 \right) I_{3 \times 3} & - \left(\frac{1}{2} \sigma_u^2 \Delta t^2 \right) I_{3 \times 3} \\ 0_{3 \times 3} & - \left(\frac{1}{2} \sigma_u^2 \Delta t^2 \right) I_{3 \times 3} & (\sigma_u^2 \Delta t) I_{3 \times 3} \end{array} \right] \quad (38)$$

It should be noted that corrected version of Eq. (38) is only an approximation, since the coupling effects of the cross-product matrix in Eq. (29) have not been considered. The approximation is valid if the sampling rate is below Nyquist's limit. Also, the process noise for the velocity is assumed to have equal levels, i.e. its covariance is a scalar ($\sigma^2 \Delta t$) times identity; however, this does not need to be required in general.

V. Colored-Noise Kalman Filter for Sensor Vibration Mitigation

In this section a colored-noise Kalman filter is developed that will be used to reduce the error effects caused by placing the VISNAV beacons on flexible structures. The vibration model for the i^{th} beacon is assumed to be given by the following form:

$$\begin{aligned} \begin{bmatrix} \dot{X}_i \\ \dot{Y}_i \\ \dot{Z}_i \\ \ddot{X}_i \\ \ddot{Y}_i \\ \ddot{Z}_i \end{bmatrix} &= \begin{bmatrix} 0 & 0 & 0 & 1 & 0 & 0 \\ 0 & 0 & 0 & 0 & 1 & 0 \\ 0 & 0 & 0 & 0 & 0 & 1 \\ -\frac{K}{M} & 0 & 0 & -\frac{C}{M} & 0 & 0 \\ 0 & -\frac{K}{M} & 0 & 0 & -\frac{C}{M} & 0 \\ 0 & 0 & -\frac{K}{M} & 0 & 0 & -\frac{C}{M} \end{bmatrix} \begin{bmatrix} X_i \\ Y_i \\ Z_i \\ \dot{X}_i \\ \dot{Y}_i \\ \dot{Z}_i \end{bmatrix} \\ &+ \begin{bmatrix} \frac{1}{M} & 0 & 0 & 0 & 0 & 0 \\ 0 & \frac{1}{M} & 0 & 0 & 0 & 0 \\ 0 & 0 & \frac{1}{M} & 0 & 0 & 0 \\ 0 & 0 & 0 & \frac{1}{M} & 0 & 0 \\ 0 & 0 & 0 & 0 & \frac{1}{M} & 0 \\ 0 & 0 & 0 & 0 & 0 & \frac{1}{M} \end{bmatrix} \begin{bmatrix} 0 \\ 0 \\ 0 \\ \eta_{X_i} \\ \eta_{Y_i} \\ \eta_{Z_i} \end{bmatrix} \end{aligned} \quad (39)$$

where X_i , Y_i and Z_i are Cartesian components of the position for the i^{th} beacon, and η_{X_i} , η_{Y_i} and η_{Z_i} are process noise terms. Here it is assumed that a simple flexible structure with isotropic matrices for the mass, damping and stiffness matrices, with scalar components respectively given by M , C and K . The vibration model can be general in nature if desired, i.e. using fully populated mass, damping and stiffness matrices, or even derived from experimental data using an algorithm such as the one shown in Ref. 27.

The aggregated state-space equation is written considering all the available beacons. This leads to a $13 + 6N$ dimensioned state vector, which includes the target position, velocity, quaternion, gyro bias, as well as the position and velocities of the flexible structure of all beacons:

$$\mathbf{x} = [\mathbf{p}^T \ \mathbf{v}^T \ \mathbf{q}^T \ \boldsymbol{\beta}^T \ \boldsymbol{\chi}_1^T \ \dot{\boldsymbol{\chi}}_1^T \ \cdots \ \boldsymbol{\chi}_N^T \ \dot{\boldsymbol{\chi}}_N^T]^T \quad (40)$$

where $\boldsymbol{\chi}_i \equiv [X_i \ Y_i \ Z_i]^T$. The Kalman filter follows along similar lines as the one shown in Table 1 with the augmented state vector in Eq. (40). The ‘‘colored-noise’’ in the system is in the beacon locations, which are used in the VISNAV measurement model. The sensitivity matrix now becomes

$$H_k(\hat{\mathbf{x}}_k^-) = \left[\begin{array}{cccccccc} \frac{\partial \hat{\mathbf{b}}_1^-}{\partial \hat{\mathbf{p}}^-} & 0_{3 \times 3} & [A(\hat{\mathbf{q}}^-)\hat{\mathbf{r}}_1^- \times] & 0_{3 \times 3} & \frac{\partial \hat{\mathbf{b}}_1^-}{\partial \hat{\boldsymbol{\chi}}_1^-} & 0_{3 \times 3} & \cdots & 0_{3 \times 3} & 0_{3 \times 3} \\ \vdots & \vdots & \vdots & \vdots & \vdots & \vdots & \cdots & \vdots & \vdots \\ \frac{\partial \hat{\mathbf{b}}_N^-}{\partial \hat{\mathbf{p}}^-} & 0_{3 \times 3} & [A(\hat{\mathbf{q}}^-)\hat{\mathbf{r}}_N^- \times] & 0_{3 \times 3} & 0_{3 \times 3} & 0_{3 \times 3} & \cdots & \frac{\partial \hat{\mathbf{b}}_N^-}{\partial \hat{\boldsymbol{\chi}}_N^-} & 0_{3 \times 3} \end{array} \right]_{t_k} \quad (41)$$

The partial matrix $\partial \hat{\mathbf{b}}_i^- / \partial \hat{\boldsymbol{\chi}}_i^-$ is given by

$$\frac{\partial \hat{\mathbf{b}}_i^-}{\partial \hat{\boldsymbol{\chi}}_i^-} = -A(\hat{\mathbf{q}}^-) \frac{\partial \hat{\mathbf{r}}_i^-}{\partial \hat{\mathbf{p}}^-} \quad (42)$$

where $\partial \hat{\mathbf{b}}_i^- / \partial \hat{\mathbf{p}}^-$ is given by Eq. (32). In this paper we consider 6 beacons. For this case the new matrix

$F(\hat{\mathbf{x}}, t)$ is given by

$$F(\hat{\mathbf{x}}, t) = \begin{bmatrix} 0_{3 \times 3} & I_{3 \times 3} & 0_{3 \times 21} & 0_{3 \times 21} \\ 0_{3 \times 12} & 0_{3 \times 12} & 0_{3 \times 12} & 0_{3 \times 12} \\ 0_{3 \times 6} & -[\boldsymbol{\omega} \times] & -I_{3 \times 3} & 0_{3 \times 36} \\ 0_{3 \times 12} & 0_{3 \times 12} & 0_{3 \times 12} & 0_{3 \times 12} \\ 0_{3 \times 15} & I_{3 \times 3} & 0_{3 \times 15} & 0_{3 \times 15} \\ 0_{3 \times 12} & -\frac{K}{M} I_{3 \times 3} & -\frac{C}{M} I_{3 \times 3} & 0_{3 \times 30} \\ 0_{3 \times 21} & I_{3 \times 3} & 0_{3 \times 12} & 0_{3 \times 12} \\ 0_{3 \times 18} & -\frac{K}{M} I_{3 \times 3} & -\frac{C}{M} I_{3 \times 3} & 0_{3 \times 24} \\ 0_{3 \times 27} & I_{3 \times 3} & 0_{3 \times 9} & 0_{3 \times 9} \\ 0_{3 \times 24} & -\frac{K}{M} I_{3 \times 3} & -\frac{C}{M} I_{3 \times 3} & 0_{3 \times 18} \\ 0_{3 \times 33} & I_{3 \times 3} & 0_{3 \times 6} & 0_{3 \times 6} \\ 0_{3 \times 30} & -\frac{K}{M} I_{3 \times 3} & -\frac{C}{M} I_{3 \times 3} & 0_{3 \times 12} \\ 0_{3 \times 39} & I_{3 \times 3} & 0_{3 \times 3} & 0_{3 \times 3} \\ 0_{3 \times 36} & -\frac{K}{M} I_{3 \times 3} & -\frac{C}{M} I_{3 \times 3} & 0_{3 \times 6} \\ 0_{3 \times 15} & 0_{3 \times 15} & 0_{3 \times 15} & I_{3 \times 3} \\ 0_{3 \times 21} & 0_{3 \times 21} & -\frac{K}{M} I_{3 \times 3} & -\frac{C}{M} I_{3 \times 3} \end{bmatrix} \quad (43)$$

The process noise vector is given by

$$\mathbf{w} = [\boldsymbol{\eta}_a^T \quad \boldsymbol{\eta}_v^T \quad \boldsymbol{\eta}_u^T \quad \boldsymbol{\eta}_{\chi_1}^T \quad \cdots \quad \boldsymbol{\eta}_{\chi_6}^T]^T \quad (44)$$

where $\boldsymbol{\eta}_{\chi_i} \equiv [\eta_{X_i} \quad \eta_{Y_i} \quad \eta_{Z_i}]^T$. It is assumed that the spectral density of each $\boldsymbol{\eta}_{\chi_i}$ is isotropic, given by $\sigma_{\chi_i}^2 I_{3 \times 3}$, for simplicity. The matrices G and Q are also augmented for the beacon location process noise:

$$G = \begin{bmatrix} 0_{3 \times 3} & \cdots & 0_{3 \times 3} & 0_{3 \times 3} \\ I_{3 \times 3} & 0_{3 \times 3} & \cdots & 0_{3 \times 3} & 0_{3 \times 3} \\ 0_{3 \times 3} & -I_{3 \times 3} & 0_{3 \times 3} & \cdots & 0_{3 \times 3} & 0_{3 \times 3} \\ 0_{3 \times 3} & 0_{3 \times 3} & I_{3 \times 3} & 0_{3 \times 3} & 0_{3 \times 3} & 0_{3 \times 3} & 0_{3 \times 3} & \cdots & 0_{3 \times 3} & 0_{3 \times 3} \\ 0_{3 \times 3} & \cdots & 0_{3 \times 3} & 0_{3 \times 3} \\ 0_{3 \times 3} & 0_{3 \times 3} & 0_{3 \times 3} & 0_{3 \times 3} & I_{3 \times 3} & 0_{3 \times 3} & 0_{3 \times 3} & \cdots & 0_{3 \times 3} & 0_{3 \times 3} \\ 0_{3 \times 3} & \cdots & 0_{3 \times 3} & 0_{3 \times 3} \\ 0_{3 \times 3} & I_{3 \times 3} & \cdots & 0_{3 \times 3} & 0_{3 \times 3} \\ \vdots & \ddots & \vdots & \vdots \\ 0_{3 \times 3} & \cdots & 0_{3 \times 3} & 0_{3 \times 3} \\ 0_{3 \times 3} & \cdots & 0_{3 \times 3} & I_{3 \times 3} \end{bmatrix} \quad (45)$$

and

$$Q = \begin{bmatrix} \sigma_a^2 I_{3 \times 3} & 0_{3 \times 3} & 0_{3 \times 3} & 0_{3 \times 3} & \cdots & 0_{3 \times 3} \\ 0_{3 \times 3} & \sigma_v^2 I_{3 \times 3} & 0_{3 \times 3} & 0_{3 \times 3} & \cdots & 0_{3 \times 3} \\ 0_{3 \times 3} & 0_{3 \times 3} & \sigma_u^2 I_{3 \times 3} & 0_{3 \times 3} & \cdots & 0_{3 \times 3} \\ 0_{3 \times 3} & 0_{3 \times 3} & 0_{3 \times 3} & \sigma_{\chi_1}^2 I_{3 \times 3} & \cdots & 0_{3 \times 3} \\ \vdots & \vdots & \vdots & \vdots & \ddots & \vdots \\ 0_{3 \times 3} & 0_{3 \times 3} & 0_{3 \times 3} & 0_{3 \times 3} & \cdots & \sigma_{\chi_6}^2 I_{3 \times 3} \end{bmatrix} \quad (46)$$

A closed-form solution for the state transition matrix and discrete-time process noise is intractable for the colored-noise case. If the sampling rate is within Nyquist's limit, then the following approximations can be used:

$$\Phi \approx I + \Delta t F \quad (47a)$$

$$Q \approx \Delta t G Q G^T \quad (47b)$$

If this is not true, then a numerical solution given by van Loan²⁸ can be used. First, the following matrix is formed:

$$\mathcal{A} = \begin{bmatrix} -F & G Q G^T \\ 0 & F^T \end{bmatrix} \Delta t \quad (48)$$

Then, the matrix exponential of Eq. (48) is computed:

$$\mathcal{B} = e^{\mathcal{A}} \equiv \begin{bmatrix} \mathcal{B}_{11} & \mathcal{B}_{12} \\ 0 & \mathcal{B}_{22} \end{bmatrix} = \begin{bmatrix} \mathcal{B}_{11} & \Phi^{-1} \mathcal{Q} \\ 0 & \Phi^T \end{bmatrix} \quad (49)$$

The state transition matrix is then given by

$$\Phi = \mathcal{B}_{22}^T \quad (50)$$

Also, the discrete-time process noise covariance is given by

$$\mathcal{Q} = \Phi \mathcal{B}_{12} \quad (51)$$

Since gyros usually provide measurements at a very high sampling rate, then Eq. (47) is usually adequate.

Sometimes, one or more of the optical beacons will be out of sensor field-of-view or the viewing angles between two or more beacons may be so small that a geometric singularity is encountered. For the case of intermittent data dropout, the estimation process can be continued by propagating the equations of motion or by integrating the gyro outputs corrupted by the biases. Gyro biases can be updated by the EKF even when one beacon is available in the VISNAV measurements. The VISNAV/gyro integration method can take advantage of the strengths of both systems while minimizing the impact of their weaknesses. This integration gives a robust navigation system. This navigation system provides a continuous best estimate of the dynamic system and is much more robust with respect to occasional dropouts than forward propagation using an approximate dynamic model.

The filter is first initialized with a known state and error-covariance matrix. Then, the Kalman gain is computed using the measurement-error covariance and sensitivity matrix. The state error-covariance follows the standard EKF update. Then, the error state update is computed. Based on this error state update, the position and velocity, quaternion, gyro biases, and beacon position and velocities are updated. The updated quaternion is re-normalized by brute force. Angular velocity is used to propagate the quaternion kinematics. Gyro bias and velocity propagation are constant through the sampling interval. Finally, the position and standard error-covariance are propagated in the EKF.

VI. Simulation & Results

This section presents the simulations conducted for this paper. Simulations were carried out to verify the design of the 49 state EKF. A brief introduction and discussion about the approach will be presented. Then the simulation results will be presented along with the details of the specific parameters used. The last section discusses the results obtained for the simulation.

A. Introduction and Approach

First, the colored-noise vibration model is simulated using the model in Eq. (39). Then, the measurements of $\mathbf{A} \mathbf{r}_i$ are generated for each time instant by propagating the initial identity attitude matrix with a certain angular velocity rate. Next, the gyros are simulated in discrete-time for each time instant using Eq. (11). These are the two measurements used for the design of the 49 state colored-noise EKF. The next section elaborates the major steps involved in simulating the EKF along with the various parameters used for this specific simulation.

B. Simulation Results

All the major parameters used for this simulation are shown in Table 2. The initial state is given by

$$\mathbf{x}_0 = [\mathbf{p}_0^T \ \mathbf{v}_0^T \ \mathbf{q}_0^T \ \beta_0^T \ \chi_{1_0}^T \ \cdots \ \chi_{6_0}^T]^T \quad (52)$$

where

$$\mathbf{p}_0 = [30 \ 30 \ 10]^T \text{ m} \quad (53a)$$

$$\mathbf{v}_0 = [1/10 \ 1/60 \ 1/180]^T \text{ m/s} \quad (53b)$$

$$\mathbf{q}_0 = [0 \ 0 \ 0 \ 1]^T \quad (53c)$$

$$\boldsymbol{\beta}_0 = [0.1 \ 0.1 \ 0.1]^T \text{ deg/hr} \quad (53d)$$

The initial conditions for the beacon locations, $\boldsymbol{\chi}_{10}, \dots, \boldsymbol{\chi}_{60}$, are shown in Table 3. For the colored-noise filter all initial variables are set to their true values, since with 6 beacons it is possible to obtain good position and attitude estimates using a least-squares approach, except for the gyros biases, which are set to zero. The initial covariance is set to

$$P_0 = \begin{bmatrix} (0.01)^2 I_{3 \times 3} & \mathbf{0}_{3 \times 15} & \mathbf{0}_{3 \times 15} & \mathbf{0}_{3 \times 15} \\ \mathbf{0}_{3 \times 3} & (0.0001)^2 I_{3 \times 3} & \mathbf{0}_{3 \times 3} & \mathbf{0}_{3 \times 3} \\ \mathbf{0}_{3 \times 6} & (0.1 \frac{\pi}{180})^2 I_{3 \times 3} & \mathbf{0}_{3 \times 3} & \mathbf{0}_{3 \times 3} \\ \mathbf{0}_{3 \times 9} & (0.2 \frac{\pi}{180 \times 3600})^2 I_{3 \times 3} & \mathbf{0}_{3 \times 3} & \mathbf{0}_{3 \times 3} \\ \mathbf{0}_{3 \times 12} & (0.01)^2 I_{3 \times 3} & \mathbf{0}_{3 \times 3} & \mathbf{0}_{3 \times 3} \\ \mathbf{0}_{3 \times 15} & (0.0001)^2 I_{3 \times 3} & \mathbf{0}_{3 \times 3} & \mathbf{0}_{3 \times 3} \\ \mathbf{0}_{3 \times 18} & (0.01)^2 I_{3 \times 3} & \mathbf{0}_{3 \times 3} & \mathbf{0}_{3 \times 3} \\ \mathbf{0}_{3 \times 21} & (0.0001)^2 I_{3 \times 3} & \mathbf{0}_{3 \times 3} & \mathbf{0}_{3 \times 3} \\ \mathbf{0}_{3 \times 24} & (0.01)^2 I_{3 \times 3} & \mathbf{0}_{3 \times 3} & \mathbf{0}_{3 \times 3} \\ \mathbf{0}_{3 \times 27} & (0.0001)^2 I_{3 \times 3} & \mathbf{0}_{3 \times 3} & \mathbf{0}_{3 \times 3} \\ \mathbf{0}_{3 \times 30} & (0.01)^2 I_{3 \times 3} & \mathbf{0}_{3 \times 3} & \mathbf{0}_{3 \times 3} \\ \mathbf{0}_{3 \times 33} & (0.0001)^2 I_{3 \times 3} & \mathbf{0}_{3 \times 3} & \mathbf{0}_{3 \times 3} \\ \mathbf{0}_{3 \times 36} & (0.01)^2 I_{3 \times 3} & \mathbf{0}_{3 \times 3} & \mathbf{0}_{3 \times 3} \\ \mathbf{0}_{3 \times 39} & (0.0001)^2 I_{3 \times 3} & \mathbf{0}_{3 \times 3} & \mathbf{0}_{3 \times 3} \\ \mathbf{0}_{3 \times 39} & \mathbf{0}_{3 \times 3} & (0.01)^2 I_{3 \times 3} & \mathbf{0}_{3 \times 3} \\ \mathbf{0}_{3 \times 21} & \mathbf{0}_{3 \times 21} & \mathbf{0}_{3 \times 3} & (0.0001)^2 I_{3 \times 3} \end{bmatrix} \quad (54)$$

The quaternion is updated and propagated as described in the attitude determination portion of §V. Then the sensitivity matrix H_k is calculated, shown by Eq. (42). This is an 18×48 matrix. Next the Kalman gain is calculated. The process noise matrix Q is shown in Eq. (46). The quantity σ_a is changed to tune the EKF.

C. Discussion

The colored-noise estimation results discussed in the section use a value of $K = 1$ for the stiffness in the beacon structure. This gives a natural frequency of 0.3162 rad/sec and a damping ratio of 0.1118. Figure 2(a) shows the errors (estimated minus true values) in the target vehicle's position (x , y and z components) with 3σ outliers. The errors lie within their respective 3σ outliers, which indicates that the colored-noise EKF working properly. Figure 2(b) shows the error in the target vehicle's velocity. Again, the errors lie within their respective 3σ outliers. Figure 3(a) shows the roll, pitch and yaw errors of the target vehicle. Figure 3(b) shows the x , y and z components of the gyro bias with 3σ outliers, which are slowly decreasing. Clearly, more attitude motion is required to estimate the gyro biases faster. Still good attitude estimates are provided for the simulation comparisons, which are more relevant for the study in this paper. Figure 4(a) and 4(b) show the position and velocity errors of beacon one, respectively. Similar type of results are obtained for the position and velocity errors of the remaining beacons. All these errors fall within the 3σ outliers, confirming proper estimation.

D. Sensitivity to Process Noise

In this section, the robustness with respect to process noise of the beacons is shown. The assumed value in the filter is multiplied by some scale factor of the true value. Specifically, the process noise covariance is multiplied by 1 to 13 times in the filter to check the robustness of the state estimates to errors in the

Table 2. Simulation Parameters

Parameter Name	Symbol	Unit	Values
True Vehicle Position	x	m	$30 \exp[(-1/300)t]$
	y	m	$30 - (30/1800)t$
	z	m	$10 - (10/1800)t$
Vehicle Rotational Velocity	ω	rad/s	$\sin(3t)$ $\cos(t)$ $(360 \times 3/t_f)\pi/180$
Time Step	Δt	s	0.01
Final Time	t_f	min	1.5
Mass of Beacon Structure	M	Kg	10
Spring Constant of Beacon Structure	K	N/m	1 and 38
Damping Coefficient of Beacon Structure	C	Ns/m	$\sqrt{2}/2$
Standard Deviation (STD) for Angle Random Walk	σ_v	rad/s ^{1/2}	$\sqrt{10} \exp(-7)$
STD for Rate Random Walk	σ_u	rad/s ^{3/2}	$\sqrt{10} \exp(-10)$
STD for Vehicle Acceleration	σ_a	m/s ^{3/2}	$\sqrt{4} \exp(-2)$
STD for Each Beacon Acceleration	σ_{χ_i}	m/s ^{3/2}	$\sqrt{1} \exp(-3)$
STD for Measurement	σ_m	deg	0.02

Table 3. Beacon Location in Meters

Beacon No.	X-Location	Y-Location	Z-Location
1	0.5	0.5	0
2	-0.5	-0.5	0
3	-0.5	0.5	0
4	0.5	-0.5	0
5	0.2	0	0.1
6	0	0.2	-0.1

covariance parameters. Results from the filter using various “mistuned” values for the process noise are shown in Table 4 for target position and velocity (NA indicates a diverging filter) and are shown in Table 5 for beacon one position and velocity. Various results for the specific case of a factor of 6 are shown in Figures 5-7. Even though the process noise covariance of the beacons is multiplied by a factor of 6, good state estimates are provided. Beyond this limit however only target position estimation errors start crossing their respected 3σ outliers with the other state estimation errors being very well within their respective 3σ outliers.

E. Comparison between 13 and 49 State EKF

A comparison between the 13 and 49 state EKFs is now shown. Measurements used in both filters contain vibrational beacon error-effects. In the 13 state EKF beacon vibrations are not estimated whereas in the 49 state EKF, beacon vibrations are estimated. Simulation results are shown with a higher standard deviation in the vibration noise with $\sigma_{\chi_i} = 100 \text{ mm/s}^{3/2}$ than the previous simulation results. Also, a value of $K = 38$ for the stiffness in the beacon structure is used for the comparisons. This gives a natural frequency of 1.9494 rad/sec and a damping ratio of 0.0181. Hence, the vibration effects in this simulation comparison are more pronounced than in the previous results. Plots of the results using the 13 state EKF are shown in Figures

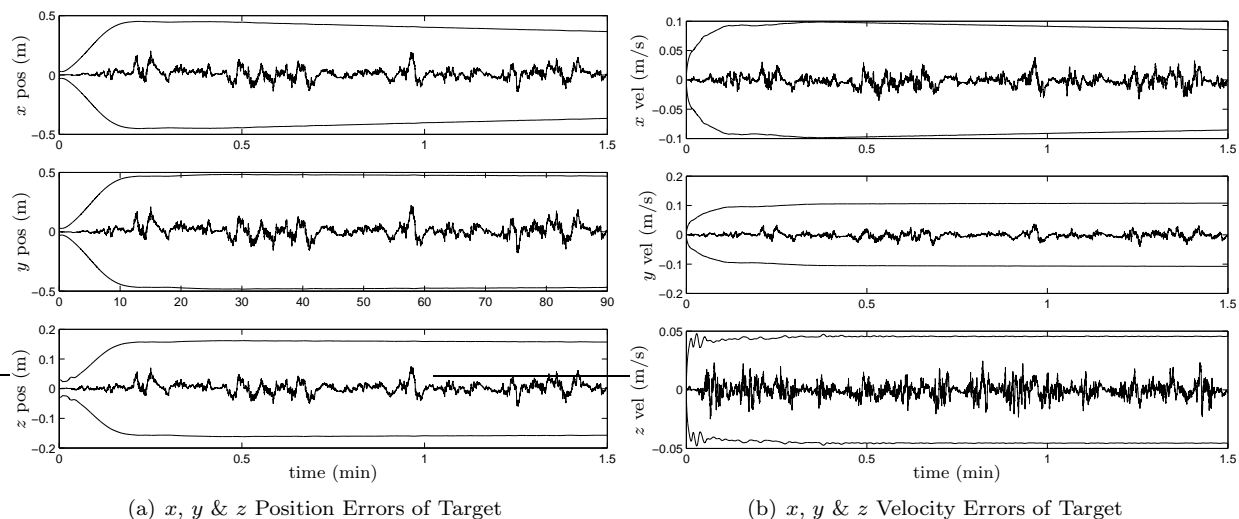


Figure 2. x , y & z Errors in Position and Velocity with 3σ Outliers for Target

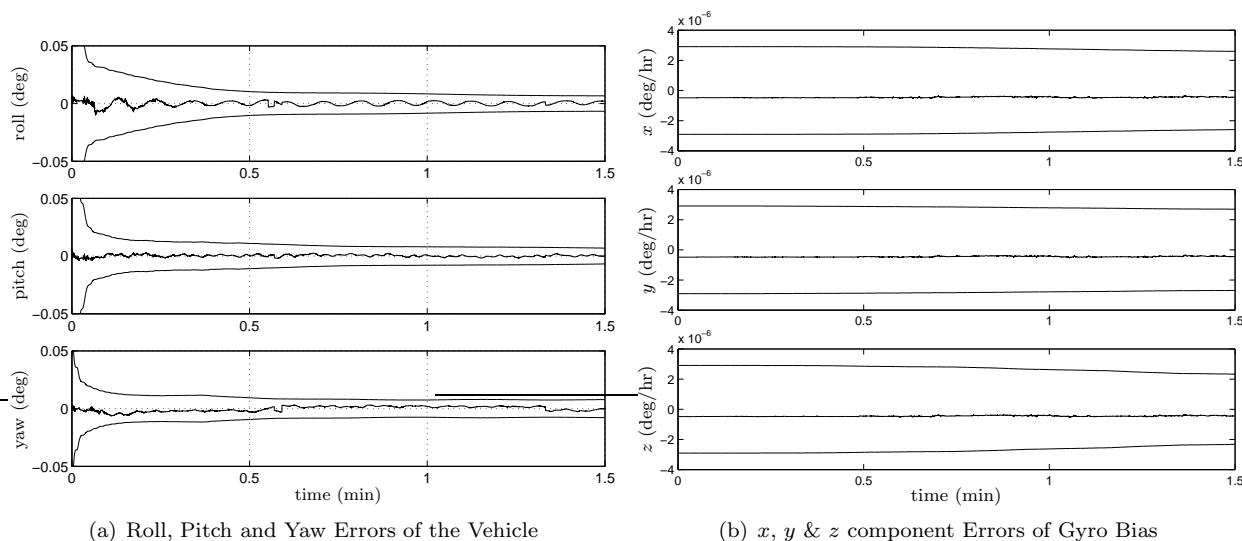
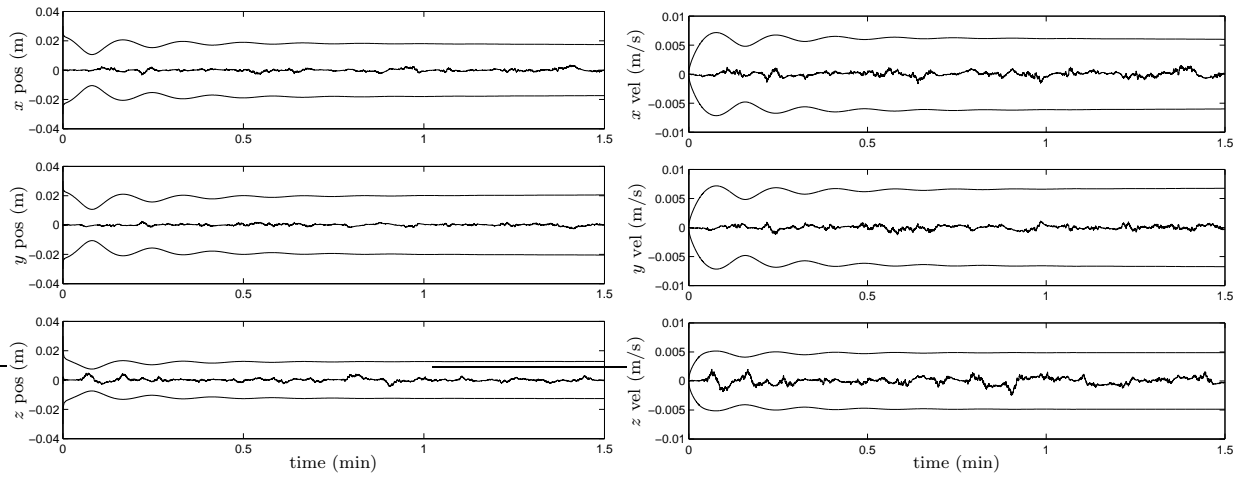


Figure 3. Roll, Pitch, Yaw Errors of the Vehicle and Gyro Bias with 3σ Outliers

8 and 9. With the exception of the gyro-bias errors, all errors are significantly outside their respective 3σ outliers. From Figure 8(a) the frequency of the oscillation in the errors corresponds to the frequency of the vibration in the beacons, which intuitively makes sense since the effect of the beacon vibrations is not compensated in the 13 state EKF. Plots of the results using the 49 state EKF are shown in Figures 10 and 11. Clearly, for same set of parameter values, the colored-noise 49 state EKF is significantly better than the 13 state EKF. This simulation comparison indicates that vibration error-effects in a sensor can be successfully mitigated using a colored-noise model in the EKF.

VII. Conclusions

This paper showed a design of a colored-noise Kalman filter for the purpose of mitigating errors associated with sensor movements in position/attitude estimation systems. The particular application of this approach involved a visual-based navigation sensor that provides a line-of-sight vector between beacons and the target. Simulation results showed that the colored-noise filter is fairly robust to errors in the assumed process noise covariance. Furthermore, the colored-noise filter showed significant improvements in both accuracy and



(a) x , y & z Position Errors of Beacon One

(b) x , y & z Velocity Errors of Beacon One

Figure 4. x , y & z Errors in Position and Velocity with 3σ Outliers for Beacon One

Table 4. Target Position and Velocity 3σ Variation with Process Noise Variation in EKF

Scale	Target Position 3σ			Target Velocity 3σ		
	x	y	z	x	y	z
1	0.4161	0.4780	0.1601	0.0932	0.1065	0.0455
2	0.6825	0.7839	0.2626	0.1106	0.1271	0.0514
3	0.9189	1.0553	0.3534	0.1226	0.1412	0.0555
4	1.1337	1.3022	0.4364	0.1318	0.1523	0.0592
5	1.3299	1.5269	0.5120	0.1390	0.1610	0.0626
6	1.5110	1.7347	0.5816	0.1452	0.1682	0.0651
7	1.6753	1.9240	0.6452	0.1499	0.1740	0.0676
8	NA	NA	NA	0.1793	0.0705	0.1400
9	NA	NA	NA	0.1840	0.0725	0.1572
10	NA	NA	NA	0.1618	0.1882	0.0745
11	NA	NA	NA	0.1638	0.1914	0.0772
12	NA	NA	NA	0.1674	0.1950	0.0786
13	NA	NA	NA	NA	NA	NA

obtaining accurate 3σ outliers than a Kalman filter running without sensor movement estimation. The approach in this paper can easily be modified for other sensor systems, where the main position and/or attitude sensor is vibrating on a flexible structure.

References

- ¹Gomez, S., "Flying High: GPS on the International Space Station and Crew Return Vehicle," *GPS World*, Vol. 13, No. 6, June 2002, pp. 12–16.
- ²Farrell, J. and Barth, M., *The Global Positioning System and Inertial Navigation*, McGraw-Hill, New York, NY, 1999.
- ³DeSouza, G. N. and Kak, A. C., "Vision for Mobile Robot Navigation: A Survey," *IEEE Transactions on Pattern Analysis and Machine Intelligence*, Vol. 24, No. 2, Feb. 2002, pp. 237–267.
- ⁴Howard, R. T., Bryan, T. C., and Book, M. L., "Video Guidance Sensor Flight Experiment Results," *Proceedings of SPIE, Laser Radar Technology and Applications III*, edited by G. W. Kamerman, Vol. 3380, Sept. 1998, pp. 315–326.
- ⁵Gupta, N. K. and Hall, W. E., "Design and Evaluation of Sensor Systems for State and Parameter Estimation," *Journal*

Table 5. Beacon One Position and Velocity 3σ Variation with Process Noise Variation in KF

Scale	Beacon One Position 3σ			Beacon One Velocity 3σ		
	x	y	z	x	y	z
1	0.0183	0.0200	0.0126	0.0061	0.0065	0.0048
2	0.0356	0.0392	0.0240	0.0120	0.0129	0.0091
3	0.0531	0.0585	0.0355	0.0178	0.0191	0.0133
4	0.0706	0.0779	0.0469	0.0235	0.0254	0.0173
5	0.0881	0.0972	0.0581	0.0292	0.0316	0.0212
6	0.1055	0.1164	0.0692	0.0348	0.0378	0.0251
7	0.1228	0.1357	0.0801	0.0405	0.0440	0.0289
8	0.1400	0.1548	0.0909	0.0461	0.0502	0.0326
9	0.1572	0.1740	0.1014	0.0516	0.0563	0.0363
10	0.1743	0.1930	0.1117	0.0572	0.0624	0.0398
11	0.1913	0.2120	0.1219	0.0627	0.0685	0.0433
12	0.2083	0.2310	0.1318	0.0682	0.0746	0.0468
13	0.2252	0.2499	0.1417	0.0736	0.0806	0.0502

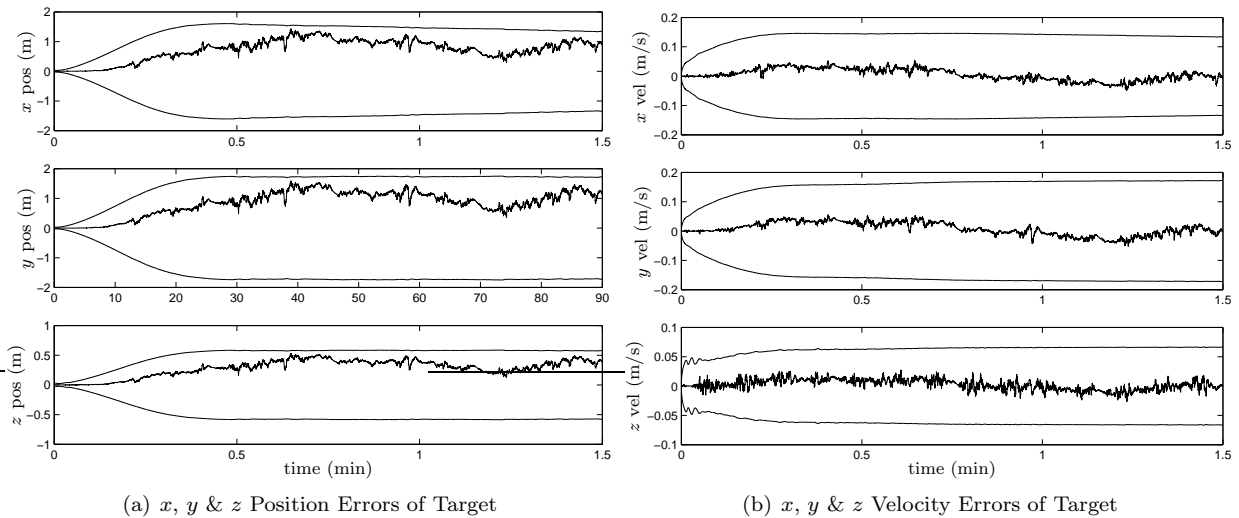


Figure 5. x , y & z Errors in Position and Velocity with 3σ Outliers for Target (Factor of 6 for Beacon Process Noise)

of *Guidance and Control*, Vol. 1, No. 6, Nov.-Dec. 1978, pp. 397–403.

⁶Chmielewski, D. J., Palmer, T., and Manousiouthakis, V., “On the Theory of Optimal Sensor Placement,” *AICHE Journal*, Vol. 48, No. 5, May 2002, pp. 1001–1012.

⁷Maquin, D., Luong, M., and Ragot, J., “Observability Analysis and Sensor Placement,” *Proceedings of the IFAC/IMACS Symposium on Fault Detection, Supervision and Safety for Technical Processes Safeprocess*, Espoo, Finland, June 1994.

⁸Sun, D. and Crassidis, J. L., “Observability Analysis of Six-Degree-of-Freedom Configuration Determination Using Vector Observations,” *Journal of Guidance, Control, and Dynamics*, Vol. 25, No. 6, Nov.-Dec. 2002, pp. 1149–1157.

⁹Ketchum Silverman, E., *Autonomous Navigation Recovery for Fine Pointing Low Earth Orbiting Spacecraft*, Ph.D. Dissertation, George Washington University, 1998.

¹⁰Cohen, C. E., Parkinson, B. W., and McNally, B. D., “Flight Tests of Attitude Determination Using GPS Compared Against an Inertial Navigation Unit,” *Navigation: Journal of the Institute of Navigation*, Vol. 41, No. 1, 1994, pp. 83–97.

¹¹Crassidis, J. L. and Junkins, J. L., *Optimal Estimation of Dynamic System*, chap. 5, Chapman & Hall/CRC, Boca Raton, FL, 2004.

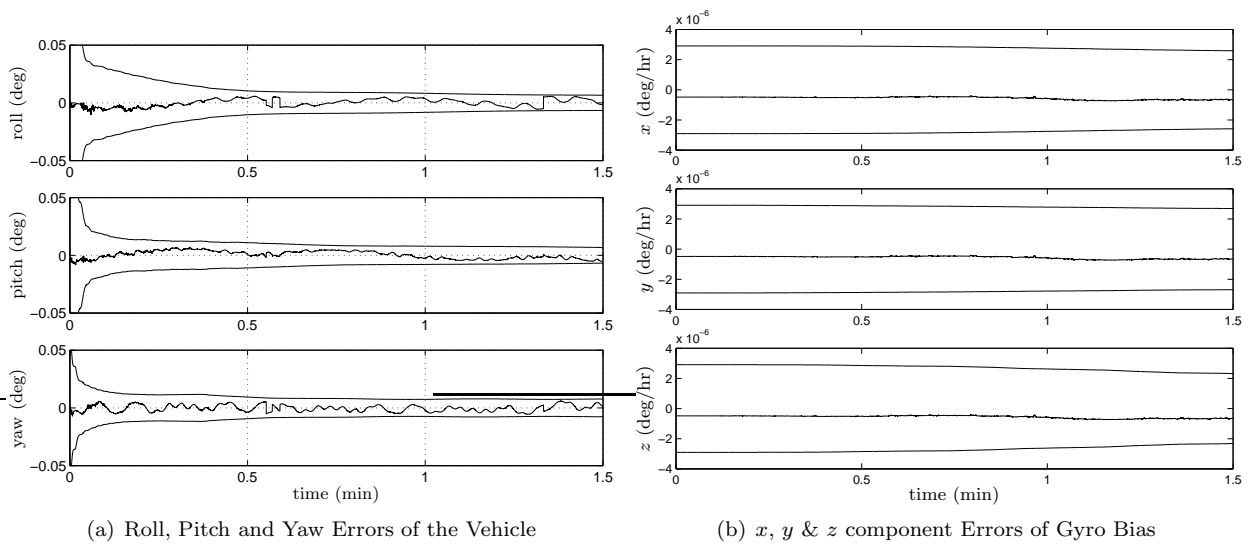


Figure 6. Roll, Pitch, Yaw Errors of the Vehicle and Gyro Bias with 3σ Outliers (Factor of 6 for Beacon Process Noise)

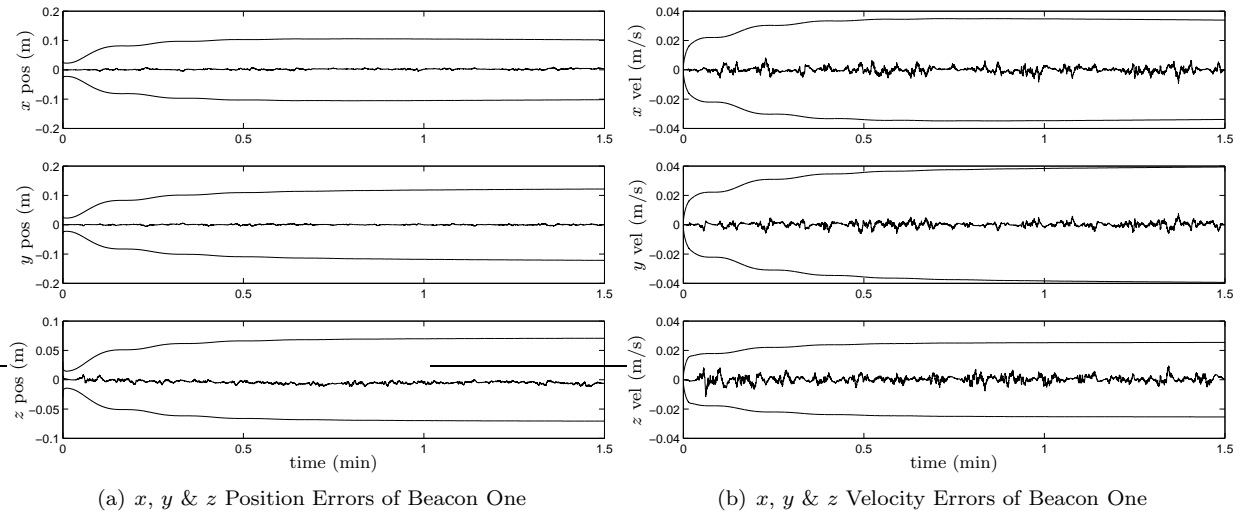


Figure 7. x , y & z Errors in Position and Velocity with 3σ Outliers for Beacon One (Factor of 6 for Beacon Process Noise)

¹²Junkins, J. L., Hughes, D., Wazni, K., and Parriyapong, V., "Vision Based Navigation for Rendezvous, Docking and Proximity Operations," *22nd Annual AAS Guidance and Control Conference*, Breckenridge CO, Feb. 1999, AAS 99-021.

¹³Gunman, K., Hughes, D., Junkins, J., and Kehtarnaraz, N., "A Vision Based DSP Embedded Navigation Sensor," *IEEE Journal of Sensors*, Vol. 2, No. 5, October 2002, pp. 428–442.

¹⁴Kim, S.-G., Crassidis, J. L., Cheng, Y., Fosbury, A. M., and Junkins, J. L., "Kalman Filtering for Relative Spacecraft Attitude and Position Estimation," *Journal of Guidance, Control, and Dynamics*, Vol. 30, No. 1, Jan.-Feb. 2007, pp. 133–143.

¹⁵Valasek, J., Kimmet, J., Hughes, D., Gunman, K., and Junkins, J., "Vision Based Sensor and Navigation System for Autonomous Aerial Refueling," *AIAA 1st Technical Conference and Workshop on Unmanned Aerospace Vehicles, Technologies and Operations*, May 2002, Portsmouth, VA.

¹⁶Light, D. L., "Satellite Photogrammetry," *Manual of Photogrammetry*, edited by C. C. Slama, chap. 17, American Society of Photogrammetry, Falls Church, VA, 4th ed., 1980.

¹⁷Cheng, Y., Crassidis, J. L., and Markley, F. L., "Attitude Estimation for Large Field-of-View Sensors," *AAS Malcolm D. Shuster Astronautics Symposium*, Grand Island, NY, June 2005, AAS-05-462.

¹⁸Shuster, M. D., "Kalman Filtering of Spacecraft Attitude and the QUEST Model," *The Journal of the Astronautical Sciences*, Vol. 38, No. 3, July-Sept. 1990, pp. 377–393.

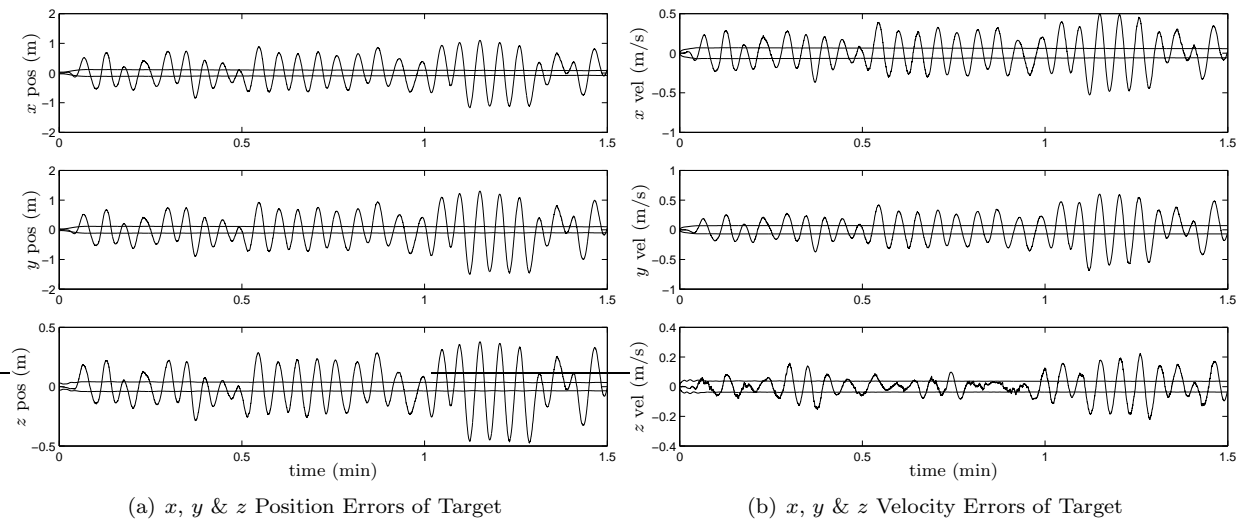


Figure 8. x , y & z Errors in Position and Velocity with 3σ Outliers for Target (13 State EKF, $\sigma_{\chi_i} = 100 \text{ mm/s}^{3/2}$)

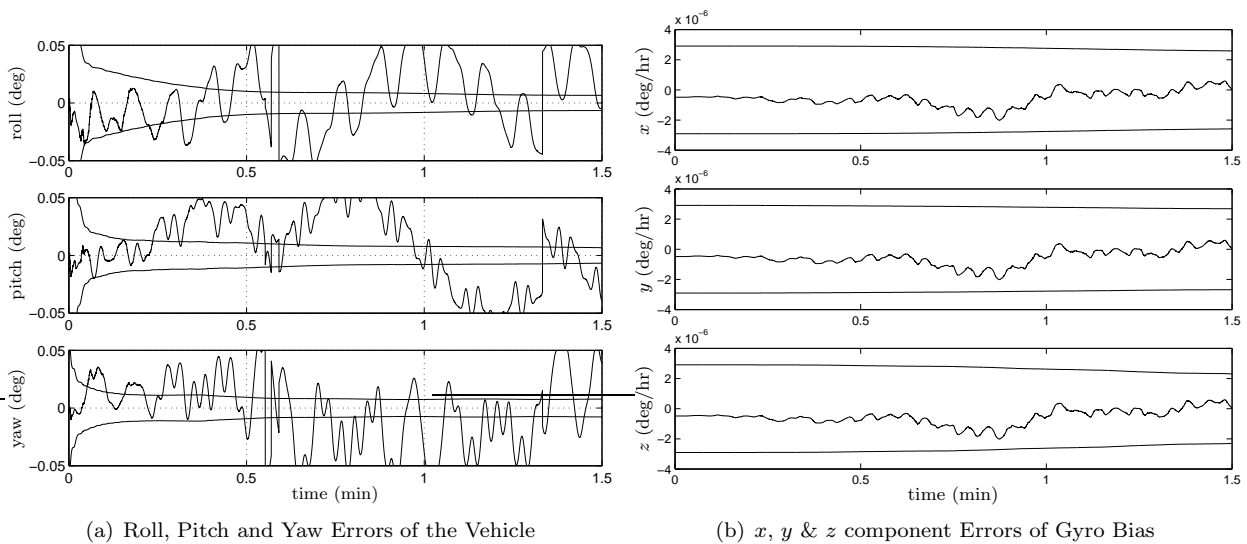


Figure 9. Roll, Pitch, Yaw Errors of the Vehicle and Gyro Bias with 3σ Outliers (13 State EKF, $\sigma_{\chi_i} = 100 \text{ mm/s}^{3/2}$)

¹⁹Shuster, M. D. and Oh, S. D., "Three-Axis Attitude Determination from Vector Observations," *Journal of Guidance and Control*, Vol. 4, No. 1, Jan.-Feb. 1981, pp. 70–77.

²⁰Farrenkopf, R. L., "Analytic Steady-State Accuracy Solutions for Two Common Spacecraft Attitude Estimators," *Journal of Guidance and Control*, Vol. 1, No. 4, July-Aug. 1978, pp. 282–284.

²¹Crassidis, J. L., "Sigma-Point Kalman Filtering for Integrated GPS and Inertial Navigation," *AIAA Guidance, Navigation, and Control Conference*, Aug. 2005, San Francisco, CA, AIAA-05-6052.

²²Shuster, M., "A Survey of Attitude Representations," *The Journal of the Astronautical Sciences*, Vol. 41, No. 4, Oct.-Dec 1993, pp. 439–517.

²³Lefferts, E. J., Markley, F. L., and Shuster, M. D., "Kalman Filtering for Spacecraft Attitude Estimation," *Journal of Guidance, Control and Dynamics*, Vol. 5, No. 5, Sept.-Oct. 1982, pp. 417–429.

²⁴Hamilton, W. R., *Elements of Quaternions*, Longmans, Green and Co., London, England, 1866.

²⁵Crassidis, J. L., Markley, F. L., and Cheng, Y., "A Survey of Nonlinear Attitude Estimation Methods," *Journal of Guidance, Control, and Dynamics*, Vol. 30, No. 1, Jan.-Feb. 2007, pp. 12–28.

²⁶Markley, F. L., "Matrix and Vector Algebra," *Spacecraft Attitude Determination and Control*, edited by J. R. Wertz, appendix C, Kluwer Academic Publishers, The Netherlands, 1978.

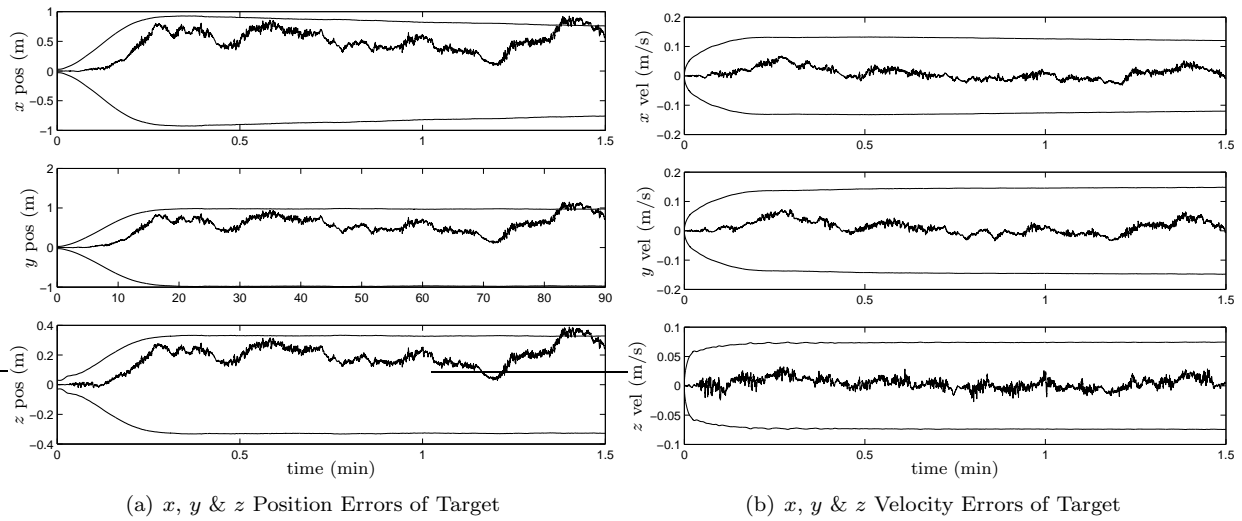


Figure 10. x , y & z Errors in Position and Velocity with 3σ Outliers for Target (49 State EKF, $\sigma_{\chi_i} = 100 \text{ mm/s}^{3/2}$)

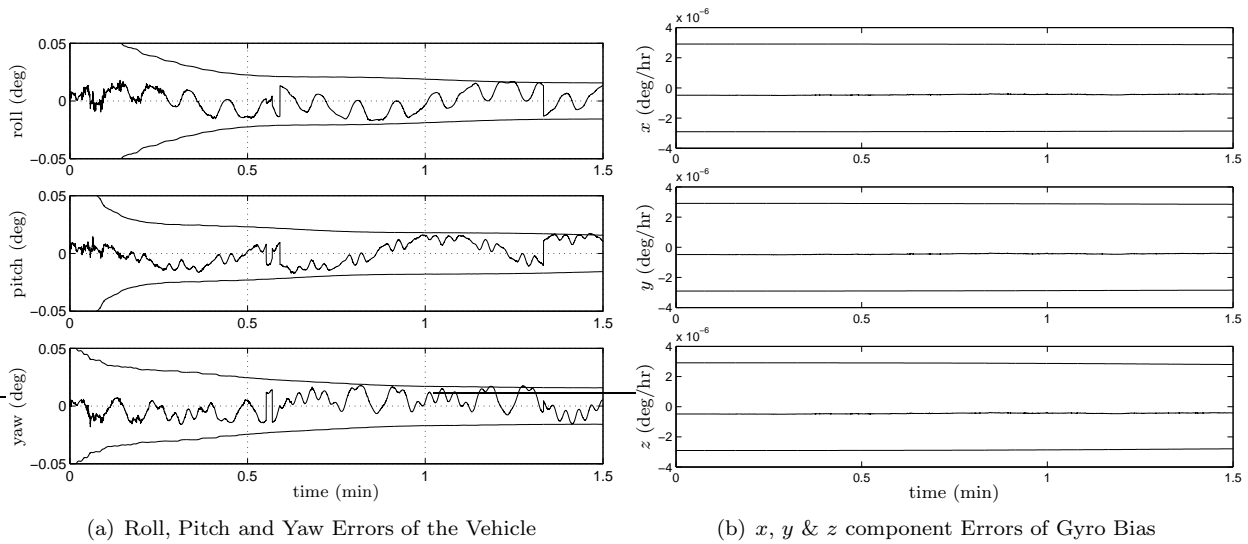


Figure 11. Roll, Pitch, Yaw Errors of the Vehicle and Gyro Bias with 3σ Outliers (49 State EKF, $\sigma_{\chi_i} = 100 \text{ mm/s}^{3/2}$)

²⁷Juang, J.-N. and Pappa, R. S., "An Eigensystem Realization Algorithm for Modal Parameter Identification and Model Reduction," *Journal of Guidance, Control, and Dynamics*, Vol. 8, No. 5, Sept.-Oct. 1985, pp. 620–627.

²⁸van Loan, C. F., "Computing Integrals Involving the Matrix Exponential," *IEEE Transactions on Automatic Control*, Vol. AC-23, No. 3, June 1978, pp. 396–404.